Cellular/Molecular Neuroscience
Senior Editor: Dr. David J. Perkel
Reviewing Editor: Dr. Catherine Woolley

Strategically positioned inhibitory synapses of axo-axonic cells potently control principal neuron spiking in the basolateral amygdala

Judit M. Veres[1,2], Gergő Attila Nagy[1], Viktória Krisztina Vereczki[1] and Norbert Hájos[1]

[1]'Lendület' Laboratory of Network Neurophysiology, Institute of Experimental Medicine, Hungarian Academy of Sciences, Budapest 1083, Hungary, [2] János Szentágothai School of Neurosciences, Semmelweis University, Budapest 1085, Hungary

Running title: Arrangement of AAC output synapses along AISs.

Keywords: GABA, interneuron, action potential, axon initial segment, mouse

Number of pages: 41
Number of figures: 6
Number of words for Abstract: 227
Number of words for Introduction: 487
Number of words for Discussion: 1495

Contact: **Norbert Hájos**
Institute of Experimental Medicine
Hungarian Academy of Sciences
Budapest H-1450, Hungary
Phone: 36-1-2109400/387
Fax: 36-1-2109412
Email: hajos@koki.hu

Acknowledgements. The authors are grateful to Péter Somogyi and Tamás F. Freund for their helpful comments on the manuscript. This work is supported by a fellowship of the Hungarian Academy of Sciences awarded to NH (Lendület, LP2012-23) and the National Office for Research and Technology (OMFB-01678/2009). VKV is supported by a European Research Council Advanced Grant (ERC-2011-ADG-294313, SERRACO). Support from these foundations is greatly acknowledged. We also thank Karri Lamsa for his advice with perforated patch recordings and Szabolcs Káli to help in analysis. The authors are grateful to Erzsébet Gregori and Éva Krizsán for their excellent technical assistance. We also thank László Barna, the Nikon Microscopy Center at the Institute of Experimental Medicine, Nikon Austria GmbH, and Auro-Science Consulting, Ltd., for kindly providing microscopy support. The authors declare no competing financial interests.

Abstract

Axo-axonic cells (AACs) in cortical regions selectively innervate the axon initial segments (AIS) of principal cells (PC), where the action potentials are generated. However, it is unknown how the output synapses of AACs relate to each other and to the exact site of action potential generation. We have addressed these questions in the mouse basolateral amygdala. Using paired recordings, we found that AACs powerfully inhibited or delayed the timing of PC spiking by 30 ms, if AAC output preceded PC spiking with no more than 80 ms. By correlating the number of synapses and the probability of spiking, we revealed that larger numbers of presynaptic AAC boutons giving rise to larger postsynaptic responses provided more effective inhibition of PC spiking. At least 10-12 AAC synapses, which could originate from 2-3 AACs on average, were necessary to veto the PC firing under our recording conditions. Furthermore, we determined that the threshold for the action potential generation along PC axons is the lowest between 15 and 30 μm from soma, which axonal segment received the highest density of GABAergic inputs. Single AACs preferentially innervated this narrow portion of the AIS where action potentials were generated with the highest likelihood, regardless of the number of synapses forming a given connection. Our results uncovered a fine organization of AAC innervation maximizing their inhibitory efficacy by strategically positioning synapses along the AISs.

Introduction

The proximal part of the axon, the axon initial segment (AIS) of neurons has the lowest threshold for action potential generation near the cell body (Stuart and Sakmann, 1994). Voltage-gated Na^+ channels on the AIS are present at high density (Lorincz and Nusser, 2010), which corresponds to the largest Na^+ influx into the AIS during firing, in comparison with the surrounding regions, including soma or dendrites (Fleidervish et al., 2010; Kole et al., 2008). In cortical structures, the axo-axonic cell (AAC) is a unique GABAergic interneuron type that predominantly, if not exclusively makes synapses onto the AIS of excitatory principal cells (PC) (Somogyi, 1977). AACs, via $GABA_A$ receptor-mediated conductances (Buhl et al., 1994a), can therefore have a substantial impact on cortical operation via control of spike generation. Indeed, these interneurons can inhibit or promote firing in PCs depending on several factors (Buhl et al., 1994a; Szabadics et al., 2006). In addition to their variable effects at the single cell level, AACs may distinctly impact neuronal processing by their specific recruiment during different network operations. For instance, sensory stimulation evokes several spikes in neocortical AACs earlier than in other cell types (Zhu et al., 2004). In the hippocampus, these interneurons discharge during theta rhythm at a phase when pyramidal cells fire least (Klausberger et al., 2003), but become silent during sharp wave-ripples (Viney et al., 2013), network activities thought to play a role in memory consolidation (Girardeau et al., 2009).

The basolateral complex of the amygdala (BLA) has been proposed to play a key role in emotional memory formation and decision making (LeDoux, 2000; Pape and Pare, 2010). Electron microscopic studies revealed that axon terminals immunostained for the calcium binding protein parvalbumin (PV) formed symmetrical synapses on the AIS of principal cells in

the BLA (Muller et al., 2006), suggesting the presence of AACs in this cortical region. In line with earlier studies obtained in the hippocampus or neocortex (DeFelipe et al., 1989; Katsumaru et al., 1988), PV-expressing interneurons targeting the AIS were identified in a recent *in vivo* study (Bienvenu et al., 2012), demonstrating that AACs in the BLA could be effectively activated by noxious stimulation, which suggests their role in regulating PC spiking. In spite of the recognition of AACs in the neocortex 40 years ago (Szentagothai and Arbib, 1974), it is still uncertain how effective the regulation of PC firing by single AACs is and how the distribution of AAC output synapses along the AIS relates to the action potential generation site.

In this study we examined the features of synaptic communication in monosynaptically-coupled AAC-PC pairs in slice preparations. *Post hoc* investigation of the properties underlying these connections allowed us to determine the number and the spatial distribution of synapses along the AIS. We found that AACs hyperpolarize their postsynaptic partners and maximize their inhibitory efficacy by positioning their synapses at the site of action potential generation, which enables them to effectively control PC firing.

Materials and methods

Experimental animals and slice preparation. All experiments were approved by the Committee for the Scientific Ethics of Animal Research (22.1/360/3/2011) and were carried out according to the guidelines of the institutional ethical code and the Hungarian Act of Animal Care and Experimentation (1998. XXVIII. section 243/1998, renewed in 40/2013.). Transgenic mice of both sex (P18-24) expressing enhanced green fluorescent protein (eGFP) under the control of the PV promoter (Meyer et al., 2002) were deeply anaesthetised with isoflurane and decapitated. The

brain was quickly removed and placed into ice-cold cutting solution containing (in mM): 252 sucrose, 2.5 KCl, 26 $NaHCO_3$, 1 $CaCl_2$, 5 $MgCl_2$, 1.25 NaH_2PO_4, 10 glucose, bubbled with 95 % O_2 / 5 % CO_2 (carbogen gas). Horizontal slices of 200 μm thickness containing the basolateral amygdala were prepared with a Leica VT1000S or VT1200S Vibratome (Wetzlar, Germany), and kept in an interface-type holding chamber containing artificial cerebrospinal fluid (ACSF) at 36 ºC that gradually cooled down to room temperature. ACSF contained (in mM) 126 NaCl, 2.5 KCl, 1.25 NaH_2PO_4, 2 $MgCl_2$, 2 $CaCl_2$, 26 $NaHCO_3$, and 10 glucose, bubbled with carbogen gas. *Electrophysiological recordings.* After at least one hour of incubation, slices were transferred individually into a submerged type recording chamber perfused with ACSF at 32±2 ºC with 2-3 ml/min flow rate. Recordings were performed under visual guidance using differential interference contrast microscopy (Olympus BX61W). EGFP in PV cells was excited by a UV lamp, and the fluorescence was visualized by a CCD camera (Hamamatsu Photonics, Japan). Patch pipettes were pulled from borosilicate glass capillaries with inner filament (Hilgenberg, Germany) using a DMZ-Universal Puller (Zeitz-Instrumente GmbH, Germany). For somatic whole-cell and perforated patch-clamp recordings, pipettes with 0.188 mm wall thickness were used and had a resistance of around 3-5 MΩ when filled with the intrapipette solution. K-gluconate-based intrapipette solution used in all recordings contained (in mM): 110 K-gluconate, 4 NaCl, 2 Mg-ATP, 20 HEPES, 0,1 EGTA, 0.3 GTP (sodium salt) and 10 phosphocreatine adjusted to pH 7.3 using KOH and with an osmolarity of 290 mOsm/L. For recording the presynaptic interneurons 10 mM GABA and 0.2% biocytin were added, whereas for the postsynaptic principal cell 100 μM Alexa Fluor 488 hydrazide sodium salt was included. Recordings were made with a Multiclamp 700B amplifier (Molecular Devices, Foster City, CA, USA), low-pass filtered at 2 kHz, digitized at 10 kHz and recorded with in-house data

acquisition and stimulus software (Stimulog, courtesy of Prof. Zoltán Nusser, Institute of Experimental Medicine, Hungarian Academy of Sciences, Budapest, Hungary). Recordings were analyzed with EVAN 1.3 (courtesy of Professor Istvan Mody, Department of Neurology and Physiology, UCLA, CA), the in-house analysis software SPIN 1.0.1 (courtesy of Prof. Zoltán Nusser) and Origin 8.6 (Northampton, MA). Recordings were not corrected for junction potential. To record the firing characteristics, cells were injected with 800 ms long hyperpolarizing and depolarizing square current pulses with increasing amplitudes from 10 to 600 pA. PC identity was characterized by the broad action potential waveform, accommodating firing pattern and slow afterhyperpolarzing current as well as the *post hoc* morphological analysis of their spiny dendrites. For recording postsynaptic inhibitory currents (IPSCs), the presynaptic AAC was held around a membrane potential of -65 mV in current-clamp mode, and stimulated by brief square current pulses (2 ms, 1.5–2 nA) to evoke action potentials, and the PC was clamped at a holding potential of -40 mV. Series resistance was monitored (range: 8-25 MΩ) and compensated by 65%. To record postsynaptic inhibitory potentials (IPSPs), the presynaptic cell was stimulated in the same way, and the postsynaptic PC was held in current clamp mode around -55 mV. Bridge balance was adjusted throughout the recordings.

To test the ability of AACs to inhibit PC firing, theta frequency (3.53 Hz) sinusoidal current pulses with peak-to-peak amplitudes of 30 pA and 50 pA were injected into the postsynaptic PC. The membrane potential of PCs was set (approximately around -55 mV) such to evoked a spike at the peak of the sinusoidal current pulses with the amplitude of 50 pA, but not of 30 pA. This adjustment maintained the membrane potential of PCs near the spiking threshold. One trial consisted of 7 sinusoidal waves (5x50pA and 2x30pA), repeated 10-20 times in each pair. Three action potentials at 30 Hz were evoked in the interneuron by brief square

current pulses (2 ms, 1.5–2 nA) before the 4th sinusoidal wave (50 pA) in each trial. To calculate the reduction in firing probability, the firing probability of PCs under control conditions was calculated from the average of the responses to 50 pA currents (1st, 3rd, 5th and 6th sinusoidal wave), which was compared to that obtained during the 4th cycle. To evoke firing in PCs by synaptic input, electrical stimulation of external capsule fibers was delivered via a theta glass electrode filled with ACSF using a Supertech timer and isolator (Supertech Ltd., Pécs, Hungary).

For perforated patch recordings 100 mg/ml gramicidin (Sigma) stock solution was prepared in DMSO daily and kept at 4 ºC. Before the recordings gramicidin stock solution was diluted to the concentration of 100 μg/ml in standard K-gluconate based intrapipette solution, which also contained 100 μM Alexa 488 hydrazide sodium salt and 1 mM QX-314. The solution was sonicated for a short period of time in an ultrasound bath several times before use. The tip of the pipette with 3-5 MΩ resistance was filled with gramicidin free solution and then backfilled with the gramicidin containing intrapipette solution. The series resistance was monitored throughout the experiment, and recordings were started when the resistance fell below 100 MΩ. Pipette capacitance was neutralized and bridge balance was carefully adjusted throughout the recordings. Patch rupture was detected by i) the inability to evoke action potentials with depolarizing current steps (the consequence of QX-314 diffusion into the cell), ii) with the penetration of Alexa 488 dye into the cell, or iii) sudden drop in the access resistance, and in such cases the experiment was terminated. To estimate the reversal potential of the evoked postsynaptic responses (Fig. 1*E, F*), we plotted the area (integral) of IPSPs as a function of membrane potential and obtained the value where the second order polynomial fit crossed the x axis. For comparing the reversal potential of IPSPs in perforated patch and whole-cell mode, we

compared the responses from the same presynaptic AAC onto a PC recorded in perforated patch mode and a neighboring PC recorded in whole-cell mode.

For simultaneous somatic and axonal bleb whole-cell measurements, PCs were recorded at the soma with K-gluconate based intrapipette solution containing 100 μM Alexa 488 and the dye filled axon blebs were visualized with a CCD camera. Then, the identified axon bleb was patched with a pipette filled with the same solution, but containing 2% biocytin (0.315 mm wall thickness, ~12 MΩ open tip resistance). Data was low-pass filtered at 20 kHz, digitally sampled at 100 kHz and analyzed with EVAN 1.3 software. Access resistance was 10-25 MΩ for somatic recordings and 30-60 MΩ for bleb recordings. Pipette capacitance was neutralized and bridge balance was adjusted throughout the recordings. Action potentials were evoked by somatic square current pulse injections (10 ms long, 0.5-2 nA at 0.5 Hz). Axonal recording distances were calculated based on the *post hoc* 3D reconstruction of the biocytin and Alexa dye labeled cells with the aid of the Neurolucida 10.53 software (MBF Bioscience).

Anatomical analysis of the synapses between AAC and PC pairs. After recordings slices were fixed in 4 % paraformaldehyde in 0.1 M phosphate buffer (PB; pH 7.4) overnight. For those slices which were processed for electron microscopic studies the fixative solution contained in addition 0.05% glutaraldehyde and 15% picric acid. Slices were then washed out with PB several times, and incubated in cryoprotective solution (30 % sucrose in 0.1 M PB) for 2 hrs, and then freeze-thawed three times above liquid nitrogen. AACs were visualized using Alexa 594 or Alexa 647-conjugated streptavidin (1:1000, Invitrogen, Carlsbad, CA, USA), whereas PCs were labeled using rabbit anti-Alexa 488 primary antibody (1:1000, Invitrogen) and Alexa 488-conjugated goat anti-rabbit secondary antibody (1:200, Invitrogen). Confocal images were collected using a Nikon A1R microscope fitted with an oil immersion apochromatic lens (CFI

Plan Apo VC60X Oil, N.A. 1.40; z step size: 0.8 μm, xy: 0.42 μm/pixel). Based on the confocal images the postsynaptic PC was fully reconstructed in 3D with the Neurolucida 10.53 software and the putative synaptic sites from the presynaptic AAC were marked. For the detailed analysis of the contacts, higher magnification images were taken with the same microscope (z step size: 0.13 μm, xy: 0.08 μm/pixel). Only those recordings were used for anatomical analysis where one presynaptic interneuron was labeled in the slice. The distribution analysis of the synapses was performed with the Neurolucida Explorer software. Values were corrected for shrinkage and flattening of the tissue (x and y axis: no correction, z axis: 1.7). Four pairs were further processed for electron microscopic studies to confirm the presence of synaptic contacts. Biocytin in AACs was visualized using avidin-biotinylated horseradish peroxidase complex reaction (ABC; Vector Laboratories, Burlingame, CA, USA) with nickel-intensified 3,3-diaminobenzidine (DAB-Ni) giving a dark brown reaction product. Alexa 488 in PCs was revealed with biotin-conjugated goat anti-rabbit antibody, with ABC reaction visualized by (3,3-diaminobenzidine) DAB giving a brown chromogen. Sections were then postfixed in 0.5 % OsO_4, treated in 10% uranyl acetate, dehydrated in a graded series of ethanol, and embedded in epoxy resin (Durcupan; Sigma). Ultrathin sections of 60 nm thickness were cut, and contact sites, where the presynaptic axon made close appositions with the identified PC or with randomly sampled targets, were analysed in serial sections.

In those experiments where the Alexa 488 labeling in PCs was insufficient for contact site analysis, cell type identity was confirmed with ankyrin G staining (Gulyas et al., 2010). Briefly, slices were re-sectioned to 40 μm thickness, and incubated in mouse anti-ankyrin G (1:100-1:500 Santa Cruz Biotechnology, Santa Cruz, CA) primary antibody and Alexa 594-conjugated goat anti-mouse secondary antibody (1:200, Invitrogen).

Reconstruction of in vivo *labeled AISs.* To get sparse labeling of PCs *in vivo*, biotinylated-dextrane amine (BDA 3kDa) was bilaterally injected with iontophoresis for 2 min into the BLA (AP: -1.8 ; ML: 3.2 ; DV: 4.0 mm from Bregma). After 2 days of recovery mice were perfused with 2.5% acrolein in 4% PFA (pH 6.8) for 10 min, the brain was removed and postfixed in 4% PFA for 1.5 hours. The areas containing the BLA were sectioned into 40 μm slices soaked in 30% sucrose overnight and the sections were kept in cryorotectant antifreeze solution consisting of sucrose, ethylene glycol, distilled H2O and phosphate-buffered saline (3:3:3.1 volume ration) at -20 C until further processing was initiated (Watson et al., 1986). Prior to immonostaining the cryoprotectant was washed out in 0.1 M PB. The sections were treated with 0.1 mg/ml pepsin (Cat. No. S3002; Dako, Glostrup, Denmark) in 1 N HCl at 37^{o}C for 15 min and washed in 0.1 M PB several times, followed by incubation in 10% normal donkey serum (NDS) containing 0.05% Triton-X 100 in 0.1 M PB for 45 min. Then, the sections were incubated in the sequentially applied primary antibodies in 0.1 M PB for four days. On the first day mouse anti-gephyrin IgG (Synaptic System 1:1000) and rabbit anti-ankyrin G IgG (Santa Cruz 1:200) were applied, incubated at 4 C°, then on the third day guinea pig anti-VGAT IgG (Frontier Institute Co.Ltd 1:1000) and goat anti-panGAD IgG (Frontier Institute Co.Ltd 1:500) were added to the solution, and further incubated at room temperature for 24 hours. The primary antibodies were visualized by the incubation of the following secondary antibodies for 2 hours at room temperature: donkey anti-mouse IgG conjugated Alexa 647, donkey anti-rabbit conjugated Dylight 405, donkey anti-guinea pig conjugated Alexa 594, donkey anti-goat conjugated Alexa 594 and Alexa 488 conjugated streptavidin. Sections were washed and mounted on slides in Vectashield (Vector Laboratories). Confocal images of the labeled cells in the BLA were collected using a Nikon A1R microscope fitted with an oil immersion apochromatic lens (z step

size: 0.13 μm, xy: 0.06 μm/pixel). To *post hoc* correct the spherical aberration, the obtained pictures were deconvolved with the aid of the Huygens software (SVI, Hilversum, The Netherlands). Based on the 3D confocal image, the AISs of the BDA labeled cells were reconstructed with the Neurolucida 10.3 software and the sites where the presynaptic boutons (i.e. panGAD/VGAT-containing profiles) faced the postsynaptic marker gephyrin, were labeled as synaptic contacts along the AISs. For the analysis of the obtained data the Neurolucida Explorer software was used. Values were corrected for shrinkage of the tissue (x, y, z axis correction: 1.08).

Nav 1.6 and ankyrin G staining of AISs. Two mice were transcardially perfused with 2% PFA in 0.2 M Na-acetate buffer (pH 6.0) for 20 min, the brain was removed and sectioned into 40 μm slices. Nav 1.6 was revealed using a polyclonal rabbit anti-Nav 1.6 (1:500, Alomone Labs) primary antibody and Alexa 488-conjugated goat anti-rabbit secondary antibody; ankyrin G was labeled as described above. Confocal images were collected with a Nikon A1R microscope (z step size: 0.13 μm, xy: 0.1 μm/pixel). For the intensity analysis of the labeling, those AISs were analyzed that run parallel to the slice surface and could be traced from the soma to the end of the labeled profile. Intensity distributions of the immunolabelings were analysed with the intensity profile function of Nikon Imaging System software using maximum z intensity projection pictures.

Statistical analysis. For comparison of data with a non-normal distribution according to theShapiro-Wilk test, the Mann-Whitney U test, Wilcoxon Signed Rank test and Kruskal-Wallis ANOVA (K-W ANOVA) was used. For the comparison of distributions, the two sample Kolmogorov-Smirnov test was used (K-S test). All statistics were performed using Origin 8.6 (Northampton, MA).. Data are presented as mean ± s.e.m. unless indicated.

Results

Axo-axonic cells innervate the axon initial segments of principal cells in the BLA

In order to study the properties of AACs in the BLA, we obtained visually-guided, targeted recordings in amygdalar slices prepared from the brains of transgenic mice expressing eGFP under the control of PV promoter (Meyer et al., 2002). After recordings, cells were morphologically identified (Fig. 1*A*) using a previously described method (Gulyas et al., 2010). Briefly, we analysed the bouton distribution of the recorded interneurons relative to the AIS of PCs at the light microscopic level. If the boutons of an interneuron formed close appositions with the AIS of the intracellularly-labeled PC in a monosynaptically-connected pair or with immunostained profiles visualized with an antibody recognizing the anchoring protein, ankyrin G (Fig. 1*B*), we identified the cell to be an AAC. In this study, 45 AACs were included after separation from other types of PV-expressing interneurons, i.e. from putative basket cells and dendrite-targeting interneurons (n=28). In the case of 3 AACs, we confirmed by electron microscopy that their axon terminals formed symmetrical synapses preferentially on AISs (n= 25 out of 28 boutons, Fig. 1*C*). Thus, in the BLA, similarly to other cortical regions (Buhl et al., 1994b; Tamas and Szabadics, 2004), AACs can be separated from additional types of PV-expressing interneurons based on clear structural criteria.

Fast and large synaptic inhibition characterizes the connections between axo-axonic cells and their targets

First, we determined the spiking features of AACs and their basic membrane properties. Upon intracellular current injection, these interneurons had a fast spiking phenotype (max. firing

frequency: 153.8±8.9 Hz, n=15), characterized by a firing with moderate accommodation (last/first inter-spike interval ratio: 2.03±0.10) and narrow spike width at half maximum amplitude (0.35±0.01 ms), as well as low input resistance (133.4±8.6 MΩ, Fig. 1*D*).

Next, we aimed to reveal the synaptic effects of AACs onto PCs. To minimize the disturbance of the ionic milieu in PCs, we carried out recordings between monosynaptically connected AAC-PC pairs when the postsynaptic PC was recorded in perforated patch mode using gramicidin in the recording pipette. A train of action potentials was evoked in the presynaptic AAC, while the resulting monosynaptic IPSPs were recorded in the PC at different membrane potentials (Fig. 1*E*). When we compared the estimated reversal potential of IPSPs and the resting membrane potential of PCs (Fig. 1*F*), we found that in the majority of cases (5 out of 7) AACs hyperpolarized their postsynaptic partner at resting membrane potential (Fig. 1*G*). In the two remaining cases when the IPSP reversal was above the resting membrane potential, these values were below the firing threshold of PCs. These data suggest that the synaptic effect of AACs onto PCs at resting membrane potential is inhibitory under our recording conditions (Fig. 1*G*). When we compared the reversal potential of IPSPs recorded in perforated patch mode to that obtained in whole-cell mode with an intrapipette solution containing 4 mM Cl^-, we found no significant difference (Fig. 1*G*, Mann-Whitney U test p=0.94). Therefore, in the following part of the study, the postsynaptic responses were recorded in whole-cell mode with an intrapipette solution containing 4 mM Cl^- concentration.

To reveal the basic characteristics of synaptic inhibition originating from AACs, AAC-PC cell pairs were recorded using the voltage-clamp configuration (Fig. 1*H, I*). We found that the probability of finding a connected pair was high (84%; n=45/54). Spikes in the presynaptic AACs triggered responses in the PCs with low failure rate (probability of failure: 0.05±0.02) and

fixed, short latency (1.01±0.03 ms, n=20), indicative of monosynaptic connections (Fig. 1*H*). The unitary postsynaptic currents recorded at a membrane potential of -40 mV had an amplitude of 100.5±13.5 pA on average, fast rise and decay kinetics (10-90% rise time: 0.83±0.07 ms; decay time constant: 6.27±0.53 ms), and were mediated via $GABA_A$ receptors, since a specific antagonist of $GABA_A$ receptors (10 μM gabazine) eliminated the action potential-evoked postsynaptic currents (n=3, data not shown). When we evoked three action potentials in AACs at 30 Hz, the amplitude of IPSCs showed a modest short-term depression (peak 3/peak 1, 0.80±0.03; n=20, Fig. 1*I*). In current clamp mode, IPSPs recorded in PCs at -55 mV upon evoking action potentials in AACs had large amplitude (1.23±0.19 mV, n=16). When three action potentials were evoked in AACs, the IPSP amplitudes showed a pronounced short-term depression (peak3/peak1, 0.49±0.04). These data show that PCs receive large and reliable synaptic inputs from AACs that are inhibitory in nature and show short-term depression.

Axo-axonic cells potently regulate principal cell spiking

In the next set of experiments, we explored how inhibitory input from an AAC can control action potential generation in a PC. PCs in the BLA display intrinsic membrane potential oscillations at theta frequency *in vivo*, a rhythm that can facilitate periodic firing at theta frequencies (Pape et al., 1998). To mimic this intrinsic oscillation, we injected a sinusoidal current at low theta frequency (3.53 Hz) and adjusted the membrane potential of the PC to spike single action potentials at the peak of the sinusoidal inputs (see Materials and methods for details). To test the effect of the synaptic inhibition onto PC firing probability, three action potentials at 30 Hz were evoked in the presynaptic AAC before the positive peak of the sinusoidal current (Fig. 2*A*). In these experiments trains of action potentials were used instead of single spikes, since AACs tend

to fire multiple spikes *in vivo* when they become active (Bienvenu et al., 2012; Klausberger et al., 2003; Massi et al., 2012; Zhu et al., 2004). The stimulation of the interneuron was timed to provide the maximal inhibitory effect at the peak of the sinusoidal current, where the PC spiked with the highest probability. We found that under these conditions AACs could significantly reduce the firing probability of PCs (79.4±5.9% reduction, n=22 cells) compared to those sinusoidal cycles when the interneuron was silent (Fig. 2*B*, K-W ANOVA $p<0.001$). The analysis showed that there was a strong positive correlation (Hill fit, $p<0.001$) between the magnitude of the synaptic inhibition (assessed as the IPSP integral, area of the IPSP under the baseline membrane potential) and the reduction in the firing probability of PCs, i.e. larger IPSPs from AACs more effectively reduced the PC spiking (Fig. 2*C*). We have estimated that an IPSP integral about 1 mV/ms is needed to achieve a 95% reduction in the PC firing probability under these conditions.

Experimental and theoretical studies show that in addition to the spiking probability, inhibitory inputs can also prominently control the timing of action potential generation, which might play an important role in cortical network functions (Cobb et al., 1995; Kwag and Paulsen, 2009). To investigate how an AAC can affect the timing of PC firing and to determine the time window in which this interneuron can control the spike generation, IPSPs were evoked at different phases of the sinusoidal current injected into PCs (Fig. 2*D*, *E*). These experiments uncovered that depending on the timing of the inhibition, AACs could delay the generation of spikes in PCs with a minimum and maximum delay of 9.69±1.37 ms and 27.3±1.45 ms (n=8), respectively, defining a significant spike timing control within a time window of 20 ms. A controlling effect on PC firing by AACs was detected even if the peak of IPSPs was 79.5±7.03

ms before the peak of the sinusoidal current (Fig. 2*F*). Thus, AACs in the BLA, in addition to their veto of action potential generation in PCs, can substantially control the timing of PC firing.

Although the sinusoidal current protocol is a reliable and controllable method to generate action potentials in PCs, spikes during physiological operation are evoked mainly by incoming integrated synaptic inputs (Epsztein et al., 2010; Svoboda et al., 1997). To test if AACs are also able to inhibit excitatory postsynaptic potential-evoked action potentials, we stimulated the fibers in the external capsule of the amygdala to induce synaptic input-driven single spikes in PCs (Fig. 2*G*). In the absence of AAC activity, the electrical stimulation of fibers readily evoked spikes in PCs, which was significantly reduced when three action potentials were evoked in a single presynaptic AAC at 30 Hz (63.6±7.9% reduction, ANOVA $p<0.001$, n=12, Fig. 2*H*). These results imply that, depending on the timing of AAC activity, when AACs fire multiple action potentials, they can potently inhibit PC firing or delay their discharge.

Higher efficacy of inhibition is promoted by multiple synapses

To get deeper insights into the properties of synaptic organization underlying the potent inhibition between AACs and PCs, we first determined the number of putative synaptic sites between the recorded pairs using multichannel high resolution confocal microscopy. Specifically, we counted the number of AAC boutons that formed close appositions with the AIS of the recorded PC (visualized in red and green, respectively; Fig. 3*A-D*, see Materials and methods). This analysis uncovered that single AACs formed 8.4 ± 0.7 putative synapses on average with their postsynaptic partners (range: 2-16 boutons/AIS, total number of boutons: 201, n=24 pairs; Fig. 3*J*). We applied two approaches to confirm that the putative synaptic sites identified with confocal microscopy were synaptic junctions. First, for 6 cell pairs we visualized

a cell adhesion molecule, neuroligin 2, which is present at GABAergic synapses, (Varoqueaux et al., 2004) to identify the functional contacts at the confocal microscopic level (Fig. 3*E*). This analysis revealed that in most instances (92%, n=44/48 boutons) immunolabeling for neuroligin 2 could be identified at the close appositions formed by AAC boutons with AISs of PCs. Second, we performed correlated light and electron microscopy in four cell pairs (Fig. *3F-I*). We found that at the vast majority of boutons (96%, 28 out of 29 boutons), synapses could be unequivocally identified. These two approaches verified that in the overwhelming majority of cases, synaptic junctions underlie the contacts between AACs and PCs indentified by light microscopy. Having determined the number of synaptic contacts at AAC-PC pairs, we next correlated this parameter with the physiological properties of these connections. We observed that the number of the contacting boutons correlated with the integral of the recorded IPSPs (Fig. 3*K*). Moreover, those AACs which contacted their partner with more synapses could inhibit the action potential generation more efficiently (tested in the protocol using sinusoidal current injection; Fig. 3*L*). We calculated that to achieve a 95% reduction in PC firing probability, simultaneous input from approximately 12 boutons was needed (Hill fit $p<0.001$, Fig. 3*L*). These results revealed the high efficacy of synaptic inhibition provided by AACs and showed that it substantially depends on the number of synaptic contacts targeting the AIS of PCs.

The variability in the bouton number from a single AAC to a single PC (2-16 contacts, coefficient of variation, CV=0.45) raises the question of whether there are AACs that preferentially target their postsynaptic partners via numerous synapses, while others only make a few contacts. This would imply that some AACs might have more profound effects on PC spiking during network operation than others. Or, alternatively, the large variability in the number of boutons contacting AISs characterizes the output of each AAC. To address this

question, we counted the number of boutons of *in vitro* labeled AACs forming close appositions on 10-20 individual, randomly-sampled, ankyrin G-stained AISs. We found that each AAC contacted different AISs with a variable number of varicosities ranging from 2 to 14 (5.5±0.25, n=616 boutons from 6 AACs onto 112 AISs, Fig. 3*M*), with similar variance in the bouton number (CV range: 0.36-0.67). Since the length of the ankyrin G-labeled profiles in slices was 39.4±0.7 μm (n=112), we re-analysed the data obtained in pairs by restricting the analysis to those boutons present at the proximal part of the axon no further than 39.4 μm from the soma. This measurement allowed us to compare directly the variance in the number of boutons targeting single AISs found in ankyrin G-labeled material with those obtained in paired recordings. We found no difference in the distributions of the bouton numbers at AISs using these two methods (K-S test p=0.76, Fig. 3*N*). Thus, we confirmed that our paired recordings reliably characterize the population of AAC outputs and, more importantly, AACs form a homogenous population regarding the manner in which they contact PCs, innervating their targets via a variable number of boutons.

We also observed that the AAC boutons along the AISs were not evenly distributed. Approximately 50% of all varicosities were found between 15 and 30 μm from the soma (Fig. 3*O*). This observation suggests that a specific region along the AIS is preferentially innervated by AACs.

Distribution of inhibitory inputs along the AIS in vivo

Our data suggest that the AAC output is not homogeneously distributed along the AIS, but concentrated in a region close to PC cell bodies. To extend these results obtained in slice preparations, we reconstructed the GABAergic input arriving onto the AISs of *in vivo* labeled

PCs. Using quadruple immunostaining we analyzed the distribution of synaptic inputs along the AISs by confocal microscopy. PCs in the BLA were labeled *in vivo* with a tracer, biotinylated dextran amine (3 kDa BDA), while their AISs were identified with immunostaining for ankyrin G (Fig. 4*A*). The GABAergic inputs were visualized with a mixture of antibodies against both isoforms of the GABA synthesizing enzyme GAD (GAD65 and GAD67, panGAD) and the vesicular GABA transporter, VGAT, whereas a scaffolding protein, gephyrin, expressed specifically at inhibitory synapses, was used to label functional synaptic junctions (Fig. 4*B*). In high resolution confocal images of the *in vivo* labeled PCs, we reconstructed AISs together with GABAergic terminals that were apposed to gephyrin labeling (Fig. 4*C*). In this material, the length of the ankyrin G-labeled segments was 58.4±1.9 μm (n=7), which corresponds to the length of the AIS. The analysis showed that single AISs received 52.4 ± 7.8 inhibitory inputs on average (range: 31-86; n=7). Importantly, the spatial distribution of the GABAergic innervation observed *in vivo* was indistinguishable from that found in *in vitro* experiments (Fig. 4*D*; K-S test, p=0.57). These results support our data obtained in slices, namely, that the GABAergic innervation of the PC AIS is concentrated on a restricted region of the AISs between 15 and 30 μm measured from the PC somata (Fig. 4*D*).

GABAergic innervation of AISs overlaps with the site of the action potential generation in PCs

Our *in vitro* and *in vivo* observations that GABAergic inputs onto AISs of PCs prefer a specific area along the proximal part of the axon raise the question of how this inhibitory input relates to the site of action potential generation. If the innervated region overlaps with the site where the threshold for action potential generation is the lowest, then AACs could have a role primarily in the control of PC spiking. However, if the area along the AIS receiving the majority of

GABAergic innervation is different from the site where the threshold for action potential generation is the lowest, then AACs may rectify PC spiking by blocking action potential propagation either towards the soma or towards the distal axon depending on the spatial relationships of the two sites. To distinguish between these possibilities, we determined where the action potentials are generated by simultaneous whole-cell recordings from the soma and an axonal bleb of the same PCs (Shu et al., 2006). We evoked an action potential in the cell by injecting a square current pulse (0.5-1.5 nA, 10 ms) via the somatic electrode and measured the evoked action potentials at both recording sites (Fig. 5*A*). After the recordings the cell was visualized and reconstructed in 3D and the distance of the axon bleb from the soma was measured (see Materials and methods, Fig. 5*B*). We compared the timing of the action potentials at the two recording sites and found that the difference in the spike timing was dependent on the distance of the axonal recording site from the soma (Fig. 5*C*). In those cases where the axonal recording sites were closer to the soma than 125 μm, the action potentials were detected at the axonal recording site prior to the somatic one, indicating that the site of action potential generation was closer to the axonal electrode. In contrast, when the axonal bleb recordings were further than 125 μm from the PC soma, action potentials recorded at the soma always preceded those detected at the axon. A bilinear fit to the data showed that the maximum difference in the axon-soma latency, which likely corresponds to the site of action potential generation, was at 24.3 μm from the soma along the AIS (95% confidence interval: 17.0 and 31.7 μm, Fig. 5*C*).

To test this result obtained using dual patch recordings and have an independent estimate for the site of action potential generation, we investigated the distribution of the Nav 1.6 subtype of voltage-gated Na^+ channel, which is critical for the initiation of action potentials (Hu et al., 2009). Using confocal microscopy, we measured the fluorescence intensity of the

immunolabeling for Nav 1.6 proteins along the AIS as defined by ankyrin G-labeling (Fig. 5*D*, *E*, n=20 AIS, profile length: 61.6±1.6 μm). We found that the most intense labeling for Nav 1.6 along the AISs (10% of the highest intensity) was at 22.5 μm from the soma (median, minimum: 18.6, maximum: 27.7, Fig. 5*E*), which corresponds surprisingly well to the action potential generation site determined by the electrophysiological recordings.

As the site of the action potential generation in PCs in the BLA closely matches the area preferentially targeted by AACs, we propose that AAC output synapses are optimized to control sodium channel opening and thus PC firing.

AACs strategically position their synapses at the site of action potential generation

Our anatomical analysis of the connectivity between AACs and PCs showed that there was a great variability in the number of synaptic contacts, ranging from 2 to up to 16 connections (Fig. 3*J*, 6*A*). This raises the question of whether the synapses originating from individual AAC-PC connections with different bouton numbers distribute evenly along the entire AIS, or, alternatively, tend to target the site of action potential generation, i.e. optimizing the efficacy of their synaptic inhibition. To address this question, we examined the bouton distribution along the AIS as a function of the number of synapses. We divided the pairs into three groups based on the number of the boutons on single AISs (1-5, 6-10 or 10-16 contacts), and compared the spatial distribution of the boutons along the AISs among the groups (Fig. 6*B*). The analysis showed that all groups tended to concentrate their synapses at the action potential generation zone (Fig. 6*B*, C). Importantly, those cells contacting their partners with a few boutons restricted their output synapses to the estimated spike generation area. In contrast, the innervations of those AACs

which gave rise to more boutons, outreached the site of action potential generation, covering a significantly broader axonal area (Fig. 6*D*, ANOVA $p<0.001$).

These data show that regardless of the actual number of output synapses, AACs preferentially innervate the site of action potential generation, and maximize their inhibitory efficacy by strategically positioning their contacts along the AIS (Fig. 6*E, F*).

Discussion

We have investigated both the structural and functional organization of the output synapses of AACs in the BLA. Our major findings are as follows: (1) AACs in the BLA hyperpolarize their postsynaptic partners at resting membrane potential or near the spike threshold. (2) AACs can effectively inhibit the firing of PC and delay spike generation. (3) The AIS length is ~60 μm as estimated from immunostainings, and AACs concentrate 50% of their output synapses to the segment between 15 and 30 μm from the soma, a region corresponding to the action potential initiation site (Fig. 6*E, F*). We propose that AACs maximize their inhibitory efficacy by strategically concentrating their synaptic junctions along the AISs to effectively counteract PC Na^+ channel activation and action potential generation.

We have shown that AACs in the BLA act via a $GABA_A$ receptor-mediated Cl^- conductance and have confirmed the results of a recent *in vivo* study obtained in the BLA, showing that AACs innervated mainly the AISs (Bienvenu et al., 2012). These observations are in agreement with those found earlier in the hippocampus and neocortex (Buhl et al., 1994a; Buhl et al., 1994b; Cobb et al., 1995; Gulyás et al., 1993; Somogyi, 1977; Somogyi et al., 1982; Somogyi et al., 1983a; Soriano and Frotscher, 1989; Szabadics et al., 2006) . However, there is

still a debate as to whether AACs inhibit or excite PCs, which may depend on several factors, including the resting membrane potential of postsynaptic neurons, the reversal potential for Cl^- in the AIS or by enhancing HCO_3^- efflux from the AIS, thereby activating Kv7/KCNQ channels (Buhl et al., 1994a; Jones et al., 2014; Szabadics et al., 2006; Woodruff et al., 2011). Using gramicidin-perforated patch recordings, we found that in the majority of PCs the reversal potential of the postsynaptic responses from AACs was below both the resting membrane potential and the firing threshold of PCs. Thus, we concluded that under our experimental conditions AACs were inhibitory in the BLA, similar to results in the hippocampus (Buhl et al., 1994a; Cobb et al., 1995; Glickfeld et al., 2009). In the neocortex, AACs can excite some of their postsynaptic partners (Molnar et al., 2008; Szabadics et al., 2006), which could be dependent on the membrane potential of PCs (Woodruff et al., 2011). Similar $GABA_A$ receptor-mediated excitation of PCs was described in the BLA *in vitro*, but the type of PV-expressing interneurons giving rise to this effect has not been clarified (Woodruff et al., 2006). Further studies should address the identity of those amygdalar interneurons that might excite PCs monosynaptically via $GABA_A$ receptors.

When the earliest studies described that AACs selectively target the AISs of PCs, it was proposed that this unique target distribution allows AACs to effectively control the activity of their postsynaptic partners (Somogyi, 1977; Somogyi et al., 1983a). Indeed, we have found that AACs are well suited to regulate PC spiking, because their output synapses, regardless of the number of contacts, predominantly cover the part of the AIS where the initiation of action potentials has the largest probability as measure by electrophysiological methods and supported by immunocytochemical data (Fig. 5). Recent studies showed that both the length and the position of the AIS along the proximal part of the axon could be dynamically regulated as a

function of neuronal excitability (Grubb and Burrone, 2010; Kuba, 2012; Kuba et al., 2010). If such a mechanism operated in cortical structures, the PCs might 'escape' from the AAC driven spike control for a period of time, which might be followed by enhancing the GABAergic input at the distal segment, a hypothesis that might be tested in the future.

Both in the hippocampus and neocortex, individual fast-spiking basket and axo-axonic cells have been shown to veto PC spiking (Cobb et al., 1995; Miles et al., 1996; Tamas et al., 2004). Similar findings were reported for PV-expressing interneurons in the BLA (Woodruff and Sah, 2007). By affecting the spiking of several neurons simultaneously, fast spiking interneurons are thus in a position to synchronize the neuronal activities at low frequencies, which might contribute to the generation of the theta rhythm (Buzsaki, 2002). In addition, the bulk stimulation of inhibitory fibers can not only delay but also advance PC spiking in the CA1 hippocampal region (Kwag and Paulsen, 2009). Indeed, we found that single AACs could significantly delay the spiking in amygdalar PCs in a similar way to that observed for CA1 PCs. However, we have not observed any advancement in PC spiking upon activation of these interneurons. The reason for this could be two-fold. First, PCs in the BLA express only a modest h-current (Faber et al., 2001; Park et al., 2007). , that mediates the advancement in spiking in CA1 (Kwag and Paulsen, 2009). Second, the GABAergic cells that make synapses on the dendrites of PCs might be more suitable to activate h-current, which is expressed predominantly in PC dendrites (Lorincz et al., 2002; Magee, 1999). Our result showing that single AACs can delay PC spiking by 10 to 30 ms suggests that AACs might have a role in regulating synaptic plasticity by restricting the precise timing of principal cell spiking to a time window when the Hebbian forms of synaptic plasticity takes place. Therefore, by organizing spike times in a large ensemble of neurons (Li et al., 2004), AACs might actively contribute to spike timing-dependent plasticity in the BLA.

Our paired recordings revealed that an AAC innervated PCs via 8.4 synapses on average, which agrees remarkably well to the 8 synaptic contacts reported in the cat visual cortex (Somogyi et al., 1982). This value was higher by ~30% than that found by counting the number of varicosities of single AACs on the ankyrin G-immunopositive profiles (5.5 bouton/AIS). The reason for the higher number of boutons found on the intracellularly-labeled PCs is that the full targeted parts of the axons are visualized including those that could not be labeled by immunostaining against ankyrin G. Thus, there might be a systematic underestimation of the number of GABAergic inputs from individual AACs onto PCs, if the counting is based on the visualization of AISs by immunostaining against e.g. ankyrin G. Reconstruction of *in vivo* labeled PCs showed that an AIS received 52.4 boutons on average, ranging from 31 to 86, which is comparable to an average of 43 in cat visual cortex (Somogyi et al., 1982), and 56 in CA1 of the monkey (Somogyi et al., 1983b), but lower than found in the CA3 area of the rat (150)(Kosaka, 1980). Our values in the BLA are higher compared to those found earlier in this region using electron microscopy. In these studies, the partial reconstruction of single AISs revealed that 15-30 synapses might contact an AIS (McDonald and Betette, 2001; Muller et al., 2006). Similar studies in other cortical regions showed that the number of synapses on single AISs is quite variable, ranging from 1 to 150 depending on the area and cortical layer (Buhl et al., 1994b; DeFelipe et al., 1985; Farinas and DeFelipe, 1991; Freund et al., 1983; Kosaka, 1980; Somogyi et al., 1982; Somogyi et al., 1983b; Tamas and Szabadics, 2004). Comparative light microscopic studies also suggested substantial variability in the innervation density of AISs between different cortical areas and layers (Inda et al., 2007, 2009) and found that the cortical nuclei of the amygdala were among the regions having particularly dense AIS innervation. Because the vast majority of these GABAergic inputs probably originated from AACs (Howard

et al., 2005), it is possible that single PCs receive innervation on their AIS from at least 4 to 10 AACs. These estimations are in accord with those obtained in other cortical structures (Buhl et al., 1994a; Freund et al., 1983; Inan et al., 2013). Taking into account our calculation that approximately 12 synapses were needed for a 95% reduction in PC firing probability under our recording conditions, a simultaneous train of action potentials in 2-3 AACs could effectively block spike genesis. This implies that for the suppression of PC firing 20-50% of all AACs innervating individual PCs should discharge synchronously.

The BLA has a homologous structure to other cortical areas, thus the activity of various GABAergic interneuron types may shape neuronal processing in this brain region similarly to others (Ehrlich et al., 2009; Spampanato et al., 2011). Indeed, a recent *in vivo* study showed that there are distinct interneuron types in the BLA with cell type-specific firing modes during network activities, together with characteristic responsiveness to incoming noxious stimuli (Bienvenu et al., 2012). Particularly, AACs discharged with high fidelity to painful stimulation, which, in combination with our data, might explain the stimulus-induced GABAergic inhibition and silencing of PCs within the BLA (Windels et al., 2010). The dense innervation of neighboring PCs with strategically positioned synapses at the action potential initiation site enable AACs to powerfully modulate the firing of their postsynaptic partners with high temporal precision, a feature which might endow them with a crucial role in amygdalar network operation during fear memory processing.

Author contributions

N.H. and J.M.V. designed the experiments, J.M.V, G.A.N. and V.K.V. performed the experiments, J.M.V, G.A.N., V.K.V. and N.H. analyzed the data, J.M.V and N.H. wrote the paper.

Figure legends

Figure 1. Axo-axonic cells (AAC) in the basolateral amygdala (BLA) make synapses on the axon initial segments (AIS) and hyperpolarize their postsynaptic targets. ***A***, Maximum z intensity projection image of an *in vitro* biocytin-filled AAC. Inset: a characteristic cartridge formed by axon terminals. ***B***, Biocytin-containing boutons of an AAC (green) make close appositions (arrows) with AISs visualized with immunofluorescent staining against ankyrin G (blue). Vesicular GABA transporter (VGAT) content in axon varicosities of an AAC is indicative of a GABAergic phenotype. ***C***, Representative axon terminal of a biocytin-filled AAC forms a symmetric synapse (black arrow) onto an AIS. ***D***, AACs have fast spiking characteristics revealed by step current injection (70, 300, -100 pA). ***E***, Postsynaptic potentials (PSPs) recorded in a principal cell (PC) at different membrane potentials in gramicidin-perforated patch recordings upon a train of 10 action potentials evoked at 40 Hz in a presynaptic AAC. ***F***, The integral of the summed PSPs was calculated at each membrane potential and fitted with a second order polynomial curve to determine the reversal potential of the response. ***G***, Comparison of the firing threshold and the resting membrane potential of PCs with the reversal potential of the PSPs recorded in perforated patch mode revealed the inhibitory nature of AACs. A similar reversal potential of PSPs was obtained in whole-cell mode using an intrapipette solution containing 4 mM Cl^- (Mann Whitney U test p=0.94). ***H-I***, Representative recordings from an AAC-PC pair in whole-cell mode using 4 mM Cl^-. Ten superimposed consecutive traces in gray, average in black. ***I***, IPSCs and IPSPs in response to 3 action potentials evoked at 30 Hz show short-term depression. PP: perforated patch, WCR: whole cell recording, VC: voltage clamp, IC: current clamp. Scale bars (in μm): ***A*** 50, inset 5; ***B*** 5, 1; ***C*** 0.5.

Figure 2. AACs effectively control action potential generation in PCs. ***A***, Representative experiment testing the capability of AACs to inhibit spike generation in PCs. Sinusoidal current trains were injected into a PC to initiate firing and three action potentials were evoked at 30 Hz in the AAC 30-40 ms before the peak of the 4th cycle (for details see Materials and methods). Red arrow points to the IPSPs in the PC evoked by AAC spike trains. Voltage traces are offset slightly for clarity. ***B***, The firing probability of PCs evoked by current injection was significantly suppressed in the presence of the action potential train evoked in AACs (n=22, K-W ANOVA $p<0.001$). Columns represent mean. ***C***, The relationship between the reduction in firing probability of PCs and the size of IPSPs (Hill function fit). ***D,*** Representative experiment testing AAC ability to postpone PC firing. The timing of the evoked action potential in an AAC was systematically shifted relative to the peak of the sinusoidal current injected into the PC. Note that a shorter interval between the presynaptic action potential train and the peak of the sinusoidal input caused a larger delay in PC spiking. ***E***, The delay in PC firing as a function of the timing of synaptic inhibition in the pair shown in ***D***. Asterisks indicate significant delay in firing compared to the peak of the cycle during the control period (paired sample Wilcoxon signed rank test $p<0.05$). ***F***, Pooled data from 8 pairs. Filled and open diamonds show the average maximal delay and the average last time point with significant delay in PC firing, respectively. ***G***, Representative experiment testing the capability of AACs to suppress PC firing driven by excitatory postsynaptic potentials (EPSPs), which were evoked by electrical stimulation of fibers in the external capsule. Voltage traces are offset slightly for clarity. ***H***, The firing probability of PCs driven by EPSPs was significantly suppressed in the presence of the action potential train evoked in AACs (n=12, K-W ANOVA $p<0.001$). Columns represent mean.

Figure 3. AACs innervate the proximal part of PC axons via multiple synaptic contacts. ***A***, Maximum z intensity projection of 3D confocal image of a representative pair. Biocytin in the AAC was visualized with streptavidin-conjugated Alexa 594 (magenta) and Alexa 488 in the PC (green). ***B***, Neurolucida reconstruction of the postsynaptic PC (green) with the putative synaptic sites marked in magenta. ***C***, High power magnification of the maximum z intensity projection image of the region indicated in ***B***, showing a part of the AIS of the postsynaptic PC (green), which receives multiple boutons (arrows) from the presynaptic AAC (magenta). ***D***, 3D analysis of confocal images of three boutons enclosed in the box in panel *C* shows close appositions of the pre- and postsynaptic structures. ***E***, Verification of the functional synapses at the light microscopic level using neuroligin-2 staining. ***F-I***, Analysis of the presence of synaptic contacts between the recorded pairs using correlative light and electron microscopy. ***F***, Neurolucida reconstruction of another AAC-PC pair. ***G***, Light micrograph of the boxed region in panel ***F***.

H-I, Electron micrographs of two boutons of the presynaptic AAC indicated in panel ***G*** are shown, both of which form synaptic contacts with the AIS of the postsynaptic PC. The white arrow in ***H*** indicates an unlabelled bouton synapsing on the biocytin-labeled AIS. ***J***, Distribution of the number of the boutons obtained by light microscopy (201 putative synaptic contacts from 24 pairs). In 28 cases, the presence of a synapse was verified using electron microscopy. ***K***, Relationship between the integral of the summed IPSPs evoked by 3 action potentials and the number of synapses made by the AAC. ***L***, Correlation between the effect of AACs on PC firing tested with a sinusoidal protocol (Fig. 2*A*-*C*) and the number of axon-AIS synapses (Hill fit $p<0.001$). ***M***, Distribution of the number of boutons from *in vitro* filled AACs on ankyrin G-labeled profiles (n=6 AACs, 616 contact sites on 112 ankyrin G-immunostained profiles, black)

and AAC-PC pairs. The analysis of the varicosities was restricted to the average length obtained from the ankyrin G staining (39.4 μm) (n=24 pairs, 134 boutons, magenta). ***N***, Cumulative distributions of bouton numbers on randomly-sampled individual ankyrin G-immunostained profiles taken from 6 filled AACs (each thin black line represent data from single AACs). The average of these distributions (thick black line) compared with the pooled data of the paired recordings shows no difference (K-S test p=0.76). ***O***, Spatial distribution of the synapses along the axon obtained in paired recordings (n=24 pairs, 201 boutons). 0 μm marks the origin of the axon at the soma, data represent mean±s.e.m. Scale bars (in μm): ***A***, ***B*** and ***F*** 30; ***C*** 5; ***D***, ***E*** 1; ***G*** 10; ***H***, ***I*** 0.25.

Figure 4. Spatial distribution of GABAergic inputs along the proximal part of PC axons *in vivo.* ***A***, Representative BDA-labeled PC (green). The AIS was identified with immunostaining against ankyrin G (magenta). ***B***, Along the BDA-labeled axon, GABAergic terminals were visualized with antibodies detecting both isoforms of the GAD enzyme (GAD65 and GAD67) and the vesicular GABA transporter, VGAT. Functional contacts were revealed based on the presence of a scaffolding synaptic protein, gephyrin. Bottom panel; superimposed neurolucida reconstruction of GABAergic inputs along the given axonal segment. Arrows show the synaptic sites along the AIS, and the open arrowhead indicates a GABAergic bouton that did not target this BDA-labeled AIS. Images were taken from a single focal plane. ***C***, 3D Neurolucida reconstruction of the proximal part of the axon and a part of the soma shown in *A* (green) and the GABAergic inputs where gephyrin was present (blue spheres) forming close apposition with the axon. ***D***, Spatial distribution of GABAergic inputs along axons labeled *in vivo* (n=7 reconstructed axons, 5 μm bin size). Data represent mean±s.e.m. Scale bars (in μm): ***A***, ***C*** 25; ***B*** 2.

Figure 5. Initiation zone for action potentials in PCs in the BLA. ***A***, Representative recordings obtained simultaneously at the soma and the axonal bleb. Top: raw data; bottom: first order derivative. The peaks of the first order derivatives were used to calculate the delay between the action potentials recorded at the two sites. ***B***, After recordings, the biocytin-filled PC was reconstructed in 3D and the distance between the two recording sites was determined. ***C***, The latency difference of the action potentials recorded at the two sites plotted as a function of the distance between the corresponding recording sites (bilinear fit minimum point at -0.16 ms and 24.4 μm, 95% confidence interval: 17.02, 31.7 μm). ***D***, Double staining for Nav 1.6 and ankyrin G in the BLA. ***E***, Normalized fluorescence intensity of the immunostainings as a function of the distance along the axon (n=20 AIS). Scatter plot shows the position of the highest 10% intensity points (minimum, median and maximum position showed). Scale bar: ***B, D,*** 10 μm.

Figure 6. AACs in the BLA preferentially target the action potential initiation zone. ***A***, Spatial distribution of the boutons along the AISs obtained in individual AAC-PC pairs. Each row represents a single AIS taken from AAC-PC pairs (n=24) that are arranged as a function of increasing bouton number. Each bouton is shown as a colored dot on each AIS (green). The pairs were categorized into three groups according to the number of contacts (black dots, 1-5 contacts; red dots, 6-10; blue dots, 11-16). ***B***, The relative frequency distributions of boutons obtained in the three groups show a large correspondence. ***C***, The position of peak values of the relative frequency distributions showed no difference among the three groups (p=0.34, ANOVA). ***D***, The number of the boutons and the covered area along the AIS (e.g. the distance between the first and last boutons) significantly differed between the three groups (p<0.001, ANOVA). ***E***,

Superimposing data from distinct experiments shows that both the peak and the shape of the intensity profile obtained by Nav 1.6 staining along the AISs correspond well to the spatial distribution of the synapses found in AAC-PC pairs. The green bar shows the Nav 1.6 intensity peak, the blue bar shows the end of the ankyrin G staining, which defines the length of the AIS. ***F***, Summary scheme indicating that AACs preferentially target, and cluster at, the site of the action potential generation along the PC axon (yellow coloring) regardless of the number of synapses made by a given connection.

References

Bienvenu, T.C., Busti, D., Magill, P.J., Ferraguti, F., and Capogna, M. (2012). Cell-type-specific recruitment of amygdala interneurons to hippocampal theta rhythm and noxious stimuli in vivo. Neuron *74*, 1059-1074.

Buhl, E.H., Halasy, K., and Somogyi, P. (1994a). Diverse sources of hippocampal unitary inhibitory postsynaptic potentials and the number of synaptic release sites. Nature *368*, 823-828.

Buhl, E.H., Han, Z.S., Lőrinczi, Z., Stezhka, V.V., Karnup, S.V., and Somogyi, P. (1994b). Physiological properties of anatomically identified axo-axonic cells in the rat hippocampus. Journal of neurophysiology *71*, 1289-1307.

Buzsaki, G. (2002). Theta oscillations in the hippocampus. Neuron *33*, 325-340.

Cobb, S.R., Buhl, E.H., Halasy, K., Paulsen, O., and Somogyi, P. (1995). Synchronization of neuronal activity in hippocampus by individual GABAergic interneurons. Nature *378*, 75-78.

DeFelipe, J., Hendry, S.H., and Jones, E.G. (1989). Visualization of chandelier cell axons by parvalbumin immunoreactivity in monkey cerebral cortex. Proc Natl Acad Sci U S A *86*, 2093-2097.

DeFelipe, J., Hendry, S.H., Jones, E.G., and Schmechel, D. (1985). Variability in the terminations of GABAergic chandelier cell axons on initial segments of pyramidal cell axons in the monkey sensory-motor cortex. J Comp Neurol *231*, 364-384.

Ehrlich, I., Humeau, Y., Grenier, F., Ciocchi, S., Herry, C., and Luthi, A. (2009). Amygdala inhibitory circuits and the control of fear memory. Neuron *62*, 757-771.

Epsztein, J., Lee, A.K., Chorev, E., and Brecht, M. (2010). Impact of spikelets on hippocampal CA1 pyramidal cell activity during spatial exploration. Science *327*, 474-477.

Faber, E.S., Callister, R.J., and Sah, P. (2001). Morphological and electrophysiological properties of principal neurons in the rat lateral amygdala in vitro. Journal of neurophysiology *85*, 714-723.

Farinas, I., and DeFelipe, J. (1991). Patterns of synaptic input on corticocortical and corticothalamic cells in the cat visual cortex. I. The cell body. J Comp Neurol *304*, 53-69.

Fleidervish, I.A., Lasser-Ross, N., Gutnick, M.J., and Ross, W.N. (2010). Na+ imaging reveals little difference in action potential-evoked Na+ influx between axon and soma. Nat Neurosci *13*, 852-860.

Freund, T.F., Martin, K.A., Smith, A.D., and Somogyi, P. (1983). Glutamate decarboxylase-immunoreactive terminals of Golgi-impregnated axoaxonic cells and of presumed basket cells in synaptic contact with pyramidal neurons of the cat's visual cortex. J Comp Neurol *221*, 263-278.

Girardeau, G., Benchenane, K., Wiener, S.I., Buzsaki, G., and Zugaro, M.B. (2009). Selective suppression of hippocampal ripples impairs spatial memory. Nat Neurosci *12*, 1222-1223.

Glickfeld, L.L., Roberts, J.D., Somogyi, P., and Scanziani, M. (2009). Interneurons hyperpolarize pyramidal cells along their entire somatodendritic axis. Nat Neurosci *12*, 21-23.

Grubb, M.S., and Burrone, J. (2010). Activity-dependent relocation of the axon initial segment fine-tunes neuronal excitability. Nature *465*, 1070-1074.

Gulyás, A.I., Miles, R., Hajos, N., and Freund, T.F. (1993). Precision and variability in postsynaptic target selection of inhibitory cells in the hippocampal CA3 region. Eur J Neurosci *5*, 1729-1751.

Gulyas, A.I., Szabo, G.G., Ulbert, I., Holderith, N., Monyer, H., Erdelyi, F., Szabo, G., Freund, T.F., and Hajos, N. (2010). Parvalbumin-containing fast-spiking basket cells generate the field

potential oscillations induced by cholinergic receptor activation in the hippocampus. J Neurosci *30*, 15134-15145.

Howard, A., Tamas, G., and Soltesz, I. (2005). Lighting the chandelier: new vistas for axo-axonic cells. Trends in neurosciences *28*, 310-316.

Hu, W., Tian, C., Li, T., Yang, M., Hou, H., and Shu, Y. (2009). Distinct contributions of Na(v)1.6 and Na(v)1.2 in action potential initiation and backpropagation. Nat Neurosci *12*, 996-1002.

Inan, M., Blazquez-Llorca, L., Merchan-Perez, A., Anderson, S.A., DeFelipe, J., and Yuste, R. (2013). Dense and overlapping innervation of pyramidal neurons by chandelier cells. J Neurosci *33*, 1907-1914.

Inda, M.C., Defelipe, J., and Munoz, A. (2007). The distribution of chandelier cell axon terminals that express the GABA plasma membrane transporter GAT-1 in the human neocortex. Cereb Cortex *17*, 2060-2071.

Inda, M.C., DeFelipe, J., and Munoz, A. (2009). Morphology and distribution of chandelier cell axon terminals in the mouse cerebral cortex and claustroamygdaloid complex. Cereb Cortex *19*, 41-54.

Jones, R.T., Faas, G.C., and Mody, I. (2014). Intracellular bicarbonate regulates action potential generation via KCNQ channel modulation. J Neurosci *34*, 4409-4417.

Katsumaru, H., Kosaka, T., Heizmann, C.W., and Hama, K. (1988). Immunocytochemical study of GABAergic neurons containing the calcium-binding protein parvalbumin in the rat hippocampus. Exp Brain Res *72*, 347-362.

Klausberger, T., Magill, P.J., Marton, L.F., Roberts, J.D., Cobden, P.M., Buzsaki, G., and Somogyi, P. (2003). Brain-state- and cell-type-specific firing of hippocampal interneurons in vivo. Nature *421*, 844-848.

Kole, M.H., Ilschner, S.U., Kampa, B.M., Williams, S.R., Ruben, P.C., and Stuart, G.J. (2008). Action potential generation requires a high sodium channel density in the axon initial segment. Nat Neurosci *11*, 178-186.

Kosaka, T. (1980). The axon initial segment as a synaptic site: ultrastructure and synaptology of the initial segment of the pyramidal cell in the rat hippocampus (CA3 region). Journal of neurocytology *9*, 861-882.

Kuba, H. (2012). Structural tuning and plasticity of the axon initial segment in auditory neurons. J Physiol *590*, 5571-5579.

Kuba, H., Oichi, Y., and Ohmori, H. (2010). Presynaptic activity regulates Na+ channel distribution at the axon initial segment. Nature *465*, 1075-1078.

Kwag, J., and Paulsen, O. (2009). Bidirectional control of spike timing by GABA(A) receptor-mediated inhibition during theta oscillation in CA1 pyramidal neurons. Neuroreport *20*, 1209-1213.

LeDoux, J.E. (2000). Emotion circuits in the brain. Annual review of neuroscience *23*, 155-184.

Li, C.Y., Lu, J.T., Wu, C.P., Duan, S.M., and Poo, M.M. (2004). Bidirectional modification of presynaptic neuronal excitability accompanying spike timing-dependent synaptic plasticity. Neuron *41*, 257-268.

Lorincz, A., Notomi, T., Tamas, G., Shigemoto, R., and Nusser, Z. (2002). Polarized and compartment-dependent distribution of HCN1 in pyramidal cell dendrites. Nat Neurosci *5*, 1185-1193.

Lorincz, A., and Nusser, Z. (2010). Molecular identity of dendritic voltage-gated sodium channels. Science *328*, 906-909.

Magee, J.C. (1999). Dendritic Ih normalizes temporal summation in hippocampal CA1 neurons. Nat Neurosci *2*, 848.

Massi, L., Lagler, M., Hartwich, K., Borhegyi, Z., Somogyi, P., and Klausberger, T. (2012). Temporal Dynamics of Parvalbumin-Expressing Axo-axonic and Basket Cells in the Rat Medial Prefrontal Cortex In Vivo. J Neurosci *32*, 16496-16502.

McDonald, A.J., and Betette, R.L. (2001). Parvalbumin-containing neurons in the rat basolateral amygdala: morphology and co-localization of Calbindin-D(28k). Neuroscience *102*, 413-425.

Meyer, A.H., Katona, I., Blatow, M., Rozov, A., and Monyer, H. (2002). In vivo labeling of parvalbumin-positive interneurons and analysis of electrical coupling in identified neurons. J Neurosci *22*, 7055-7064.

Miles, R., Toth, K., Gulyás, A.I., Hajos, N., and Freund, T.F. (1996). Differences between somatic and dendritic inhibition in the hippocampus. Neuron *16*, 815-823.

Molnar, G., Olah, S., Komlosi, G., Fule, M., Szabadics, J., Varga, C., Barzo, P., and Tamas, G. (2008). Complex events initiated by individual spikes in the human cerebral cortex. PLoS biology *6*, e222.

Muller, J.F., Mascagni, F., and McDonald, A.J. (2006). Pyramidal cells of the rat basolateral amygdala: synaptology and innervation by parvalbumin-immunoreactive interneurons. J Comp Neurol *494*, 635-650.

Pape, H.C., and Pare, D. (2010). Plastic synaptic networks of the amygdala for the acquisition, expression, and extinction of conditioned fear. Physiological reviews *90*, 419-463.

Pape, H.C., Pare, D., and Driesang, R.B. (1998). Two types of intrinsic oscillations in neurons of the lateral and basolateral nuclei of the amygdala. Journal of neurophysiology *79*, 205-216.

Park, K., Lee, S., Kang, S.J., Choi, S., and Shin, K.S. (2007). Hyperpolarization-activated currents control the excitability of principal neurons in the basolateral amygdala. Biochemical and biophysical research communications *361*, 718-724.

Shu, Y., Hasenstaub, A., Duque, A., Yu, Y., and McCormick, D.A. (2006). Modulation of intracortical synaptic potentials by presynaptic somatic membrane potential. Nature *441*, 761-765.

Somogyi, P. (1977). A specific 'axo-axonal' interneuron in the visual cortex of the rat. Brain research *136*, 345-350.

Somogyi, P., Freund, T.F., and Cowey, A. (1982). The axo-axonic interneuron in the cerebral cortex of the rat, cat and monkey. Neuroscience *7*, 2577-2607.

Somogyi, P., Kisvárday, Z.F., Martin, K.A., and Whitteridge, D. (1983a). Synaptic connections of morphologically identified and physiologically characterized large basket cells in the striate cortex of cat. Neuroscience *10*, 261-294.

Somogyi, P., Smith, A.D., Nunzi, M.G., Gorio, A., Takagi, H., and Wu, J.Y. (1983b). Glutamate decarboxylase immunoreactivity in the hippocampus of the cat: distribution of immunoreactive synaptic terminals with special reference to the axon initial segment of pyramidal neurons. J Neurosci *3*, 1450-1468.

Soriano, E., and Frotscher, M. (1989). A GABAergic axo-axonic cell in the fascia dentata controls the main excitatory hippocampal pathway. Brain research *503*, 170-174.

Spampanato, J., Polepalli, J., and Sah, P. (2011). Interneurons in the basolateral amygdala. Neuropharmacology *60*, 765-773.

Stuart, G.J., and Sakmann, B. (1994). Active propagation of somatic action potentials into neocortical pyramidal cell dendrites. Nature *367*, 69-72.

Svoboda, K., Denk, W., Kleinfeld, D., and Tank, D.W. (1997). In vivo dendritic calcium dynamics in neocortical pyramidal neurons. Nature *385*, 161-165.

Szabadics, J., Varga, C., Molnar, G., Olah, S., Barzo, P., and Tamas, G. (2006). Excitatory effect of GABAergic axo-axonic cells in cortical microcircuits. Science *311*, 233-235.

Szentagothai, J., and Arbib, M.A. (1974). Conceptual models of neural organization. Neurosciences Research Program bulletin *12*, 305-510.

Tamas, G., and Szabadics, J. (2004). Summation of unitary IPSPs elicited by identified axo-axonic interneurons. Cereb Cortex *14*, 823-826.

Tamas, G., Szabadics, J., Lorincz, A., and Somogyi, P. (2004). Input and frequency-specific entrainment of postsynaptic firing by IPSPs of perisomatic or dendritic origin. Eur J Neurosci *20*, 2681-2690.

Varoqueaux, F., Jamain, S., and Brose, N. (2004). Neuroligin 2 is exclusively localized to inhibitory synapses. European journal of cell biology *83*, 449-456.

Viney, T.J., Lasztoczi, B., Katona, L., Crump, M.G., Tukker, J.J., Klausberger, T., and Somogyi, P. (2013). Network state-dependent inhibition of identified hippocampal CA3 axo-axonic cells in vivo. Nat Neurosci *16*, 1802-1811.

Watson, R.E., Jr., Wiegand, S.J., Clough, R.W., and Hoffman, G.E. (1986). Use of cryoprotectant to maintain long-term peptide immunoreactivity and tissue morphology. Peptides *7*, 155-159.

Windels, F., Crane, J.W., and Sah, P. (2010). Inhibition dominates the early phase of up-states in the basolateral amygdala. Journal of neurophysiology *104*, 3433-3438.

Woodruff, A.R., McGarry, L.M., Vogels, T.P., Inan, M., Anderson, S.A., and Yuste, R. (2011). State-dependent function of neocortical chandelier cells. J Neurosci *31*, 17872-17886.

Woodruff, A.R., Monyer, H., and Sah, P. (2006). GABAergic excitation in the basolateral amygdala. J Neurosci *26*, 11881-11887.

Woodruff, A.R., and Sah, P. (2007). Inhibition and synchronization of basal amygdala principal neuron spiking by parvalbumin-positive interneurons. Journal of neurophysiology *98*, 2956-2961.

Zhu, Y., Stornetta, R.L., and Zhu, J.J. (2004). Chandelier cells control excessive cortical excitation: characteristics of whisker-evoked synaptic responses of layer 2/3 nonpyramidal and pyramidal neurons. J Neurosci *24*, 5101-5108.

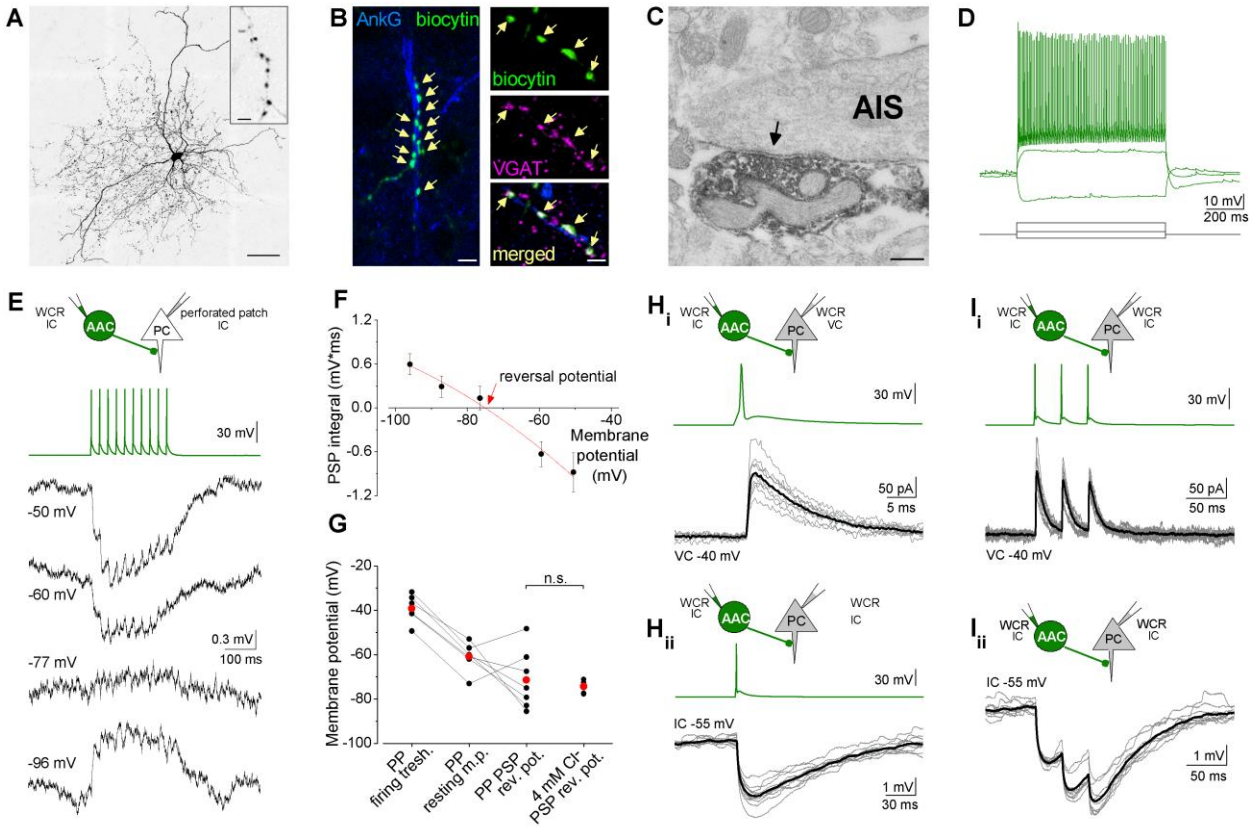
A
B
AnkG
biocytin
biocytin
VGAT
merged
C
AIS
D
10 mV
200 ms
E
WCR
IC
AAC
PC
perforated patch
IC
30 mV
-50 mV
-60 mV
0.3 mV
100 ms
-77 mV
-96 mV
F
PSP integral (mV*ms)
reversal potential
Membrane
potential
(mV)
G
Membrane potential (mV)
n.s.
PP
firing fresh.
PP
resting m.p.
PP PSP
rev. pot.
4 mM Cl-
PSP rev. pot.
Hi
WCR
VC
30 mV
50 pA
5 ms
VC -40 mV
Hii
WCR
IC
30 mV
IC -55 mV
1 mV
30 ms
Ii
30 mV
50 pA
50 ms
VC -40 mV
Iii
IC -55 mV
1 mV
50 ms

Figure 1

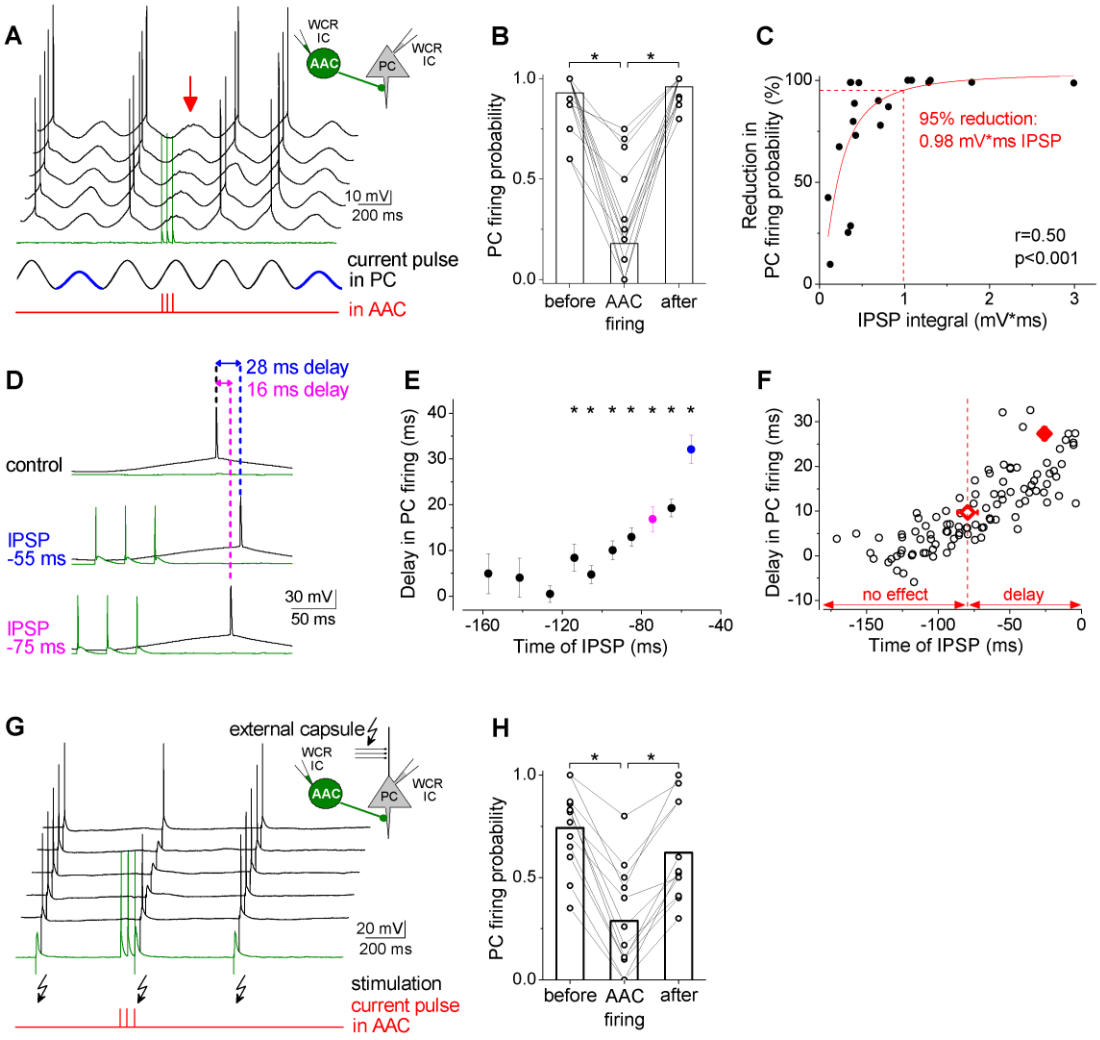
A
WCR IC
AAC
PC
WCR IC
10 mV
200 ms
current pulse in PC
in AAC
B
PC firing probability
1.0
0.5
0.0
before
AAC firing
after
C
Reduction in PC firing probability (%)
95% reduction:
0.98 mV*ms IPSP
r=0.50
p<0.001
IPSP integral (mV*ms)
D
28 ms delay
16 ms delay
control
IPSP -55 ms
IPSP -75 ms
30 mV
50 ms
E
Delay in PC firing (ms)
Time of IPSP (ms)
F
Delay in PC firing (ms)
no effect
delay
Time of IPSP (ms)
G
external capsule
WCR IC
AAC
PC
WCR IC
20 mV
200 ms
stimulation
current pulse in AAC
H
PC firing probability
before
AAC firing
after

Figure 2

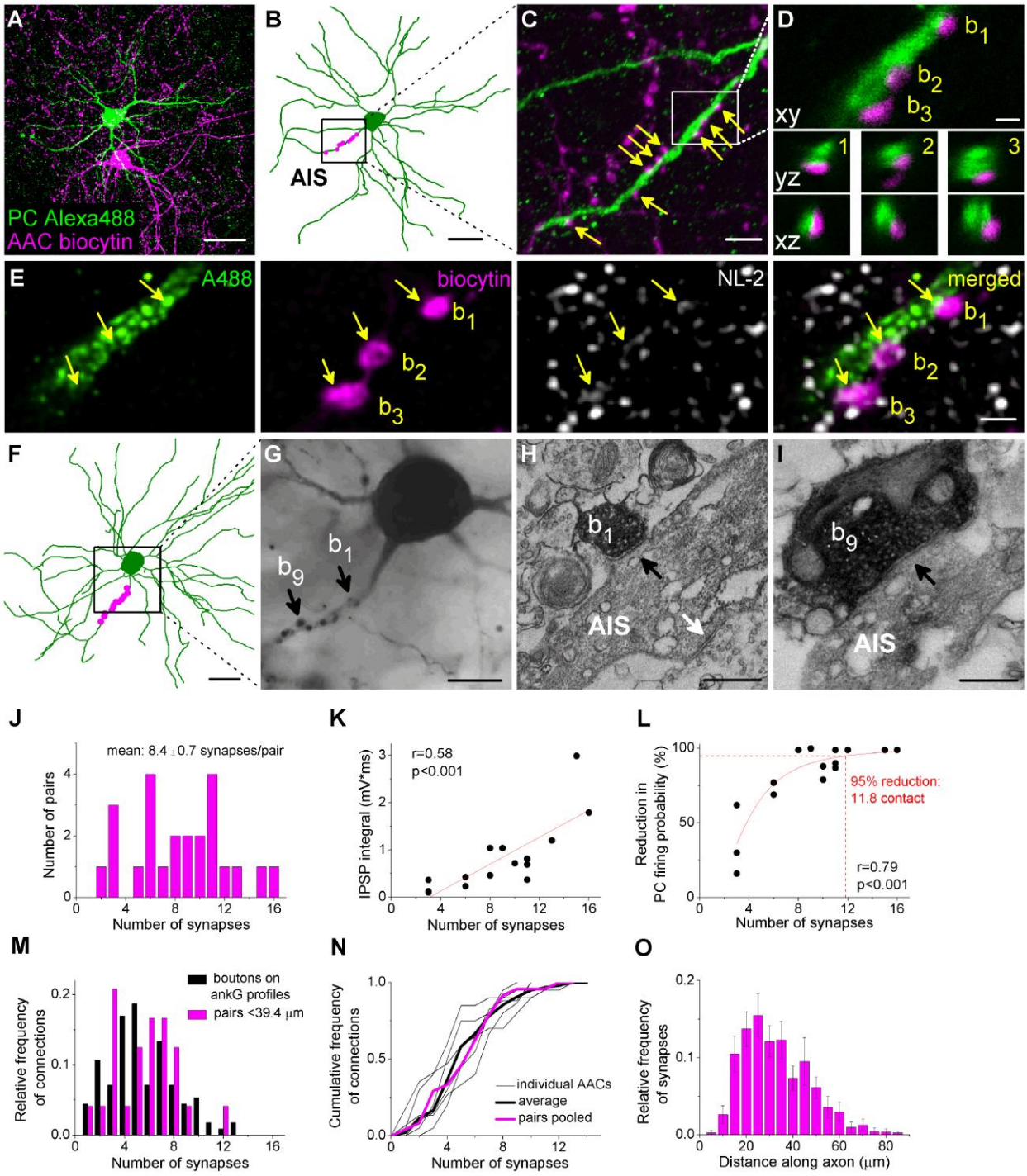
A
PC Alexa488
AAC biocytin
B
AIS
C
D
b1
b2
b3
xy
yz
xz
1
2
3
E
A488
biocytin
NL-2
merged
F
G
H
I
AIS
J
mean: 8.4 ± 0.7 synapses/pair
Number of pairs
Number of synapses
K
r=0.58
p<0.001
IPSP integral (mV*ms)
L
Reduction in PC firing probability (%)
95% reduction: 11.8 contact
r=0.79
p<0.001
M
boutons on ankG profiles
pairs <39.4 µm
Relative frequency of connections
N
Cumulative frequency of connections
individual AACs
average
pairs pooled
O
Relative frequency of synapses
Distance along axon (µm)

Figure 3

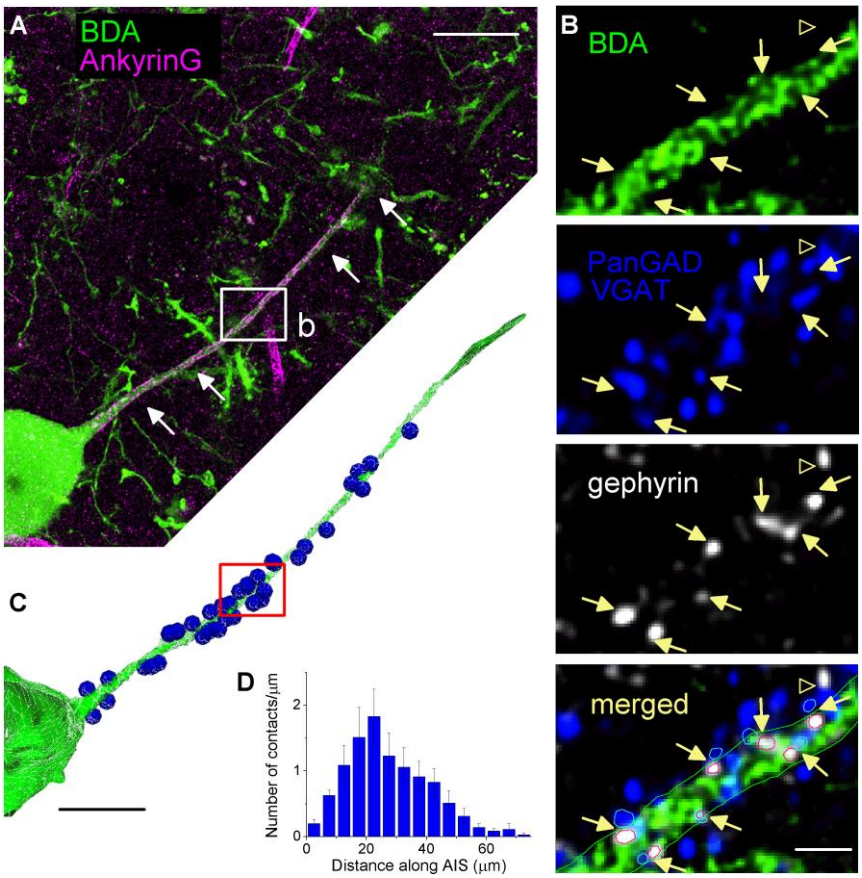
A
BDA
AnkyrinG
b
B
BDA
PanGAD
VGAT
gephyrin
merged
C
D
Number of contacts/µm
Distance along AIS (µm)
0
20
40
60
1
2

Figure 4

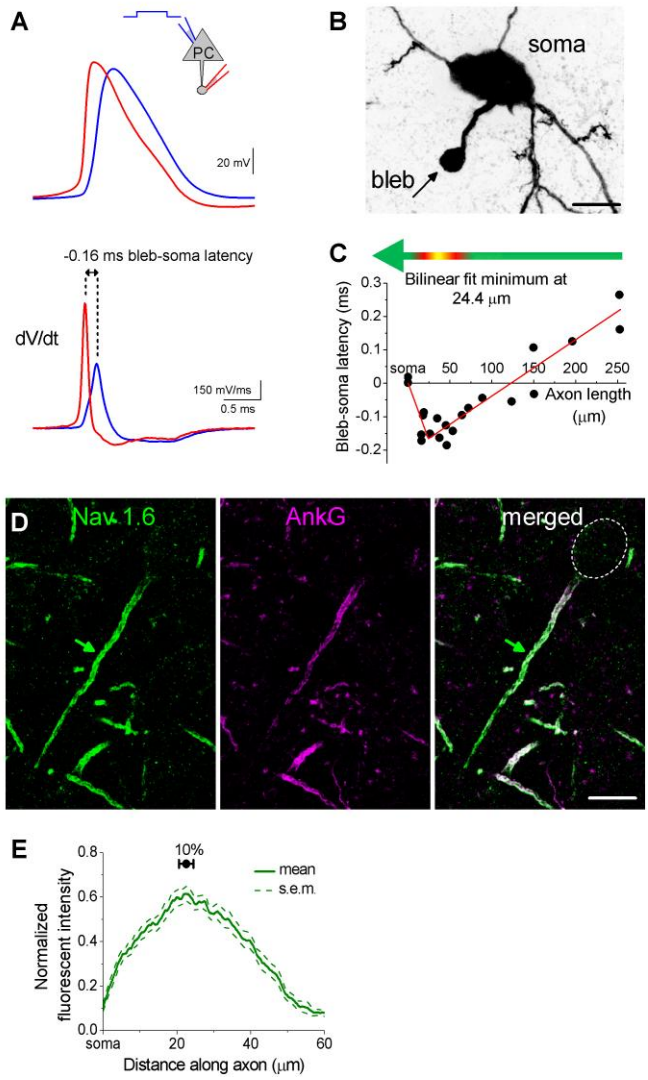
A
PC
20 mV
-0.16 ms bleb-soma latency
dV/dt
150 mV/ms
0.5 ms
B
soma
bleb
C
Bilinear fit minimum at
24.4 μm
Bleb-soma latency (ms)
0.3
0.2
0.1
0
-0.1
-0.2
soma
50
100
150
200
250
Axon length
(μm)
D
Nav 1.6
AnkG
merged
E
10%
mean
s.e.m.
Normalized
fluorescent intensity
0.8
0.6
0.4
0.2
0.0
soma
20
40
60
Distance along axon (μm)

Figure 5

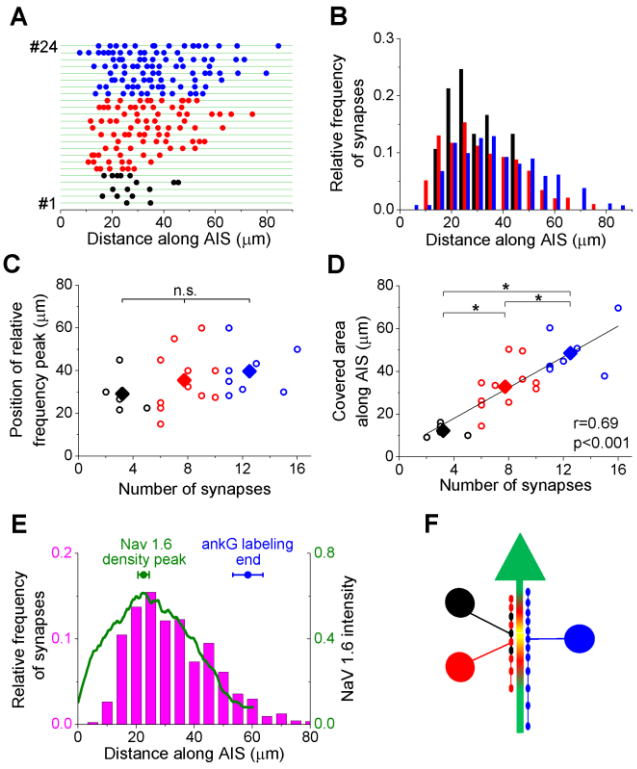
A
#24
#1
0
20
40
60
80
Distance along AIS (μm)
B
Relative frequency of synapses
0.0
0.1
0.2
0.3
Distance along AIS (μm)
C
n.s.
Position of relative frequency peak (μm)
Number of synapses
D
*
*
*
Covered area along AIS (μm)
r=0.69
p<0.001
Number of synapses
E
Nav 1.6 density peak
ankG labeling end
Relative frequency of synapses
NaV 1.6 intensity
Distance along AIS (μm)
F

Figure 6